Dynamical heterogeneity in a vapor-deposited polymer glass

Wengang Zhang,[1] Jack F. Douglas,[2] and Francis W. Starr[1]
[1]*Department of Physics, Wesleyan University, Middletown, Connecticut 06459-0155, USA*
[2]*Materials Science and Engineering Division, National Institute of Standards and Technology, Gaithersburg, Maryland 20899, USA*

(Received 13 October 2016; accepted 1 February 2017; published online 23 February 2017)

Recently, there has been great interest in "ultrastable" glasses formed via vapor deposition, both because of emerging engineering applications of these materials (e.g., active layers in light-emitting diodes and photovoltaics) and, theoretically, as materials for probing the equilibrium properties of glassy materials below their glass transition, based on the conjecture that these materials are equivalent to glassy materials aged over astronomical time scales. We use molecular dynamics simulations to examine the properties of ultrastable vapor-deposited and ordinary polymer glasses. Based on the difference in the energy of the deposited and ordinary films, we estimate the effective cooling rate for the vapor deposited films to be 1 to 3 orders of magnitude larger than that of the ordinary film, depending on the deposition temperature. Similarly, we find an increase in the average segmental relaxation time of the vapor-deposited film compared to the ordinary glass. On the other hand, the normal mode spectrum is essentially identical for the vapor-deposited and the ordinary glass film, suggesting that the high-frequency dynamics should be similar. In short, the segmental relaxation dynamics of the polymer vapor-deposited glass are consistent with those of an ordinary polymer glass with a somewhat slower effective cooling rate. Of course, one would expect a larger effect on dynamics approaching the experimental glass transition, where the cooling rates are much slower than accessible in simulation. To more precisely probe the relationship between the dynamics of these glasses, we examine dynamical heterogeneity within the film. Due to the substantial mobility gradient in the glassy films, we find that it is crucial to distinguish the dynamics of the middle part of the film from those of the entire film. Considering the film as a whole, the average dynamical heterogeneity is dominated by the mobility gradient, and as a consequence the heterogeneity is nearly indistinguishable between the ordinary and vapor deposited glass films. In contrast, in the middle part of the film, where there is almost no mobility gradient, we find the dynamical heterogeneity within the deposited film is somewhat larger than that of the ordinary film at the same temperature. We further show that the scale of the interfacial region grows on cooling in the equilibrium film, but this trend *reverses* in the glass state. We attribute this reversal in part to a shrinking ratio of the relaxation time in the middle of the film to that of the interfacial layer in the non-equilibrium state. The dynamics in this mobile interfacial layer for the ordinary and deposited film are nearly the same, suggesting that the interfacial region is always in a near-equilibrium state. These results emphasize the importance of distinguishing between interfacial and internal relaxation processes in this emerging class of materials. *Published by AIP Publishing.* [http://dx.doi.org/10.1063/1.4976542]

I. INTRODUCTION

Glasses are amorphous solids lacking the order of crystalline materials and are central to the development and utilization of emerging technologies ranging from energy storage to medical devices.[1–3] Glasses can be formed by a broad range of materials, and polymer glasses are particularly common glassy materials, due to their widespread use in the plastics industry, their occurrence in food products, and other biological materials.[4–6] The development of thin polymer films is an active area of materials' development since these films are used in many technological applications, such as micro-electronics, tissue engineering, and sensor technologies.[7–9]

Typically, glasses are prepared by rapid cooling of the liquid to avoid crystallization. Many polymers do not readily crystallize under any normal conditions, can be cooled slowly without any hint of crystallization, and transform into a glass at T_g, the glass transition temperature. Approaching T_g, the relaxation time grows rapidly with decreasing temperature so that the fluid can no longer remain in equilibrium when it is cooled faster than a rate comparable to the inverse relaxation time. Based on conventional rates of cooling in experiments, the segmental relaxation time at T_g is typically on the order of 100 s.[10] Although the relaxation time near this dynamical temperature changes very rapidly, thermodynamic quantities, such as the volume and enthalpy, show only a gradual change near T_g. The properties of glasses are dependent of the history of their preparation, since these are non-equilibrium materials.[10]

In spite of the ubiquitous applications of glasses and their occurrence in natural materials,[10–14] the fundamental description of glass formation remains one of the outstanding problems of condensed matter physics.[15] By virtue of the rapidly growing time scales required to probe equilibrium properties near T_g, experiments are normally limited

to either equilibrium properties above T_g or non-equilibrium phenomena below T_g. However, the distinguishing features of many theoretical descriptions of glass-forming liquids only arise in the predicted equilibrium behavior below the laboratory T_g.[16–22] A central theoretical and experimental challenge is to probe the nature of the equilibrium state below T_g, which is usually inaccessible due to extremely long relaxation times.

Recently, Swallen *et al.*[23] discovered that vapor deposition can be used to prepare glassy materials of small molecules that have greatly enhanced "thermal stability" characterized by a persistence of solid behavior to higher temperature than ordinary glasses (OGs) before the deposited material returns to an equilibrium fluid state. Vapor-deposited glasses exhibiting such stability are commonly referred to as "ultrastable glasses" (USGs), and it has been postulated that these USGs may be equivalent to highly aged ordinary glasses.[23–44] In such a case, USGs could offer important insights into theoretical descriptions of glass formation. The enhanced stability of USGs has obvious interest for applications, and indeed USGs have already found applications in organic light-emitting diodes (OLEDs) with display applications[45–47] and optoelectronics.[48] USGs usually have other desirable properties from an application standpoint, including higher density,[23,24,26,30,34,43,49–53] lower enthalpy,[24–26,32,33,54–57] and larger stiffness[28,58] than OGs at the same temperature. USGs made from polymeric materials have been realized using matrix-assisted pulsed laser evaporation (MAPLE),[59] although it is notable that the polymer film prepared via MAPLE has a considerably lower density than the OG. The lower density of deposited polymer glass is not considered an innate feature of polymer materials; rather, the difference is believed to arise from differences of the deposition procedure, as polymer nano-globules are deposited, rather than individual chains.[59] Thus, deposited polymer films with higher density should be possible via an alternate deposition procedure. Polymer adsorption from solution, for example, is a possibility; dense glassy layers in which polymer chains are oriented with the substrate have already been formed via the adsorption of polyelectrolytes from the solution.[60–63]

Molecular simulations of glass-forming (GF) polymer materials have offered many insights into the molecular dynamics underlying incipient glass formation in both bulk and thin film materials.[64] Recently, simulations of small molecule[27,42,53,65,66] and polymeric[67,68] vapor-deposited glasses have succeeded to generate USGs, indicating that it is possible to study these materials computationally. Much effort has been dedicated to understand the origin of the stability of USGs.[53,65,67,69] Simmons and coworkers[69] have argued that such stability is a natural consequence of the mismatch between the thermodynamic interfacial scale and dynamic gradients at the free surface.

To date, there has been scant investigation of polymeric USGs, or into the locally heterogeneous dynamics of these materials, so there is little understanding of how the dynamics of these materials might compare with that of OGs. We thus simulate polymeric USGs prepared by vapor deposition, as well as OGs, to examine the degree of dynamical heterogeneity and its variation across the film profile, and we compare the properties of these materials with those of small molecule USG materials. We confirm that our simulated polymeric and non-polymeric USG films have a dynamics and thermodynamics consistent with a range of previous experimental and simulation results, i.e., lower enthalpy, higher density, and longer relaxation time than that of the OG at the same temperature. Both the OG and USG exhibit a large mobility gradient as a function of film depth at low T. This mobility gradient is a form of dynamical heterogeneity, although this gradient is distinct from the local spatial and temporal heterogeneity of dynamics that occurs even in systems with no mobility gradient. We show that the mobility gradient can dominate traditional quantitative measures of dynamical heterogeneity. Specifically, there is little difference in dynamical heterogeneity characterized by non-Gaussian and cooperative displacements for the OG and USG as a whole. To separate the contribution of the mobility gradient to the heterogeneity in dynamics, we separately analyze the film as a whole, the interfacial region, and the middle region of the film. In contrast to the overall film, the center of the USG exhibits dynamical heterogeneity that is more pronounced than that found in the OG, consistent with the slower relaxation in the middle of the USG. We observe almost no difference between the surface dynamics of the USG and OG films. Apparently, the surface layer in both types of films persists in an equilibrium state over the entire range of temperature considered. The thickness ξ of the mobile surface layer grows on cooling in the equilibrium film, similar to the increasing scale of the cooperative motions on cooling.[70,71] However, the T dependence of ξ reverses upon entering the non-equilibrium glassy regime. This reversal has also been observed experimentally,[72] and we attribute the reversal in part to a shrinking ratio of interior to surface relaxation in the glass. To test whether our findings are specific to the polymer case, we have performed a parallel analysis on a more limited set of simulations of a small-molecule binary glass; we find the same qualitative features for the dynamical heterogeneity of the small-molecule case, suggesting that most of our findings should be applicable to USGs generally. These results emphasize that the measurement of dynamical heterogeneity for the film as a whole is not sufficient to characterize the difference in dynamical properties of OGs and USGs. These results are consistent with the possibility that the deposited film accesses lower energy states associated with the OG, and, in this sense, the USG is akin to its aged glass counterpart. That said, the formal equivalence between the USG and the aged OG is still an open question.

II. MODELING AND SIMULATION DETAILS

We use molecular dynamics simulations to study both ordinary and vapor-deposited polymer films. We model polymers as chains of 10 beads, based on the model pioneered by Kremer and Grest.[73,74] This chain length is well below the entanglement length, estimated at 30 to 60 beads (depending on the entanglement definition).[75] Non-bonded monomers interact via a Lennard-Jones (LJ) potential, truncated and shifted at 2.5σ (where σ is the LJ length parameter) so that attractive dispersion interactions are included. All units are

given relative to the strength ϵ and size σ of non-bonded polymer interactions. Consequently, T is given by ϵ/k_B, where k_B is Boltzmann's constant, and time is given in units of $(m\sigma^2/\epsilon_{mm})^{1/2}$. For a simple polymer, such as polystyrene with $T_g \approx 100\,^{\circ}$C, reduced units can be mapped to physical units with a size of chain segments $\sigma \approx 1$ nm to 2 nm, time is measured in ps, and $\epsilon \approx 1$ kJ/mol. Neighboring monomers along a chain are linked by the finitely extensible nonlinear elastic (FENE) potential[73,74] with bond stiffness $k = 30$ and range $R_0 = 1.5$, values that are known to normally preclude crystallization of the polymer fluid.

We model the substrate as a collection of LJ particles, where the LJ parameters for the possible combinations of interactions (*ss*, substrate-substrate; *ps*, polymer-substrate) are $\sigma_{ps} = 1.0$, $\epsilon_{ps} = 1.0$, $\sigma_{ss} = 0.6$, and $\epsilon_{ss} = 0.2$. We prepare a disordered substrate by randomly placing 1800 particles in a thin slice of size $20 \times 20 \times 1.2$. We use the conjugate gradient algorithm to minimize the energy and determine a structure with no net force. The substrate particles are coupled to these positions using harmonic springs of stiffness $k = 1000$. Beneath the particle substrate is a purely repulsive wall defined by a "9-3" LJ potential to constrain the lower bound of the surface.[76,77] The same substrate is used for both ordinary and deposited films. We find it necessary to use this randomly packed substrate, as opposed to a lattice arrangement, to avoid inducing crystallization of deposited films. The size of the simulated film in the plane (*xy*-direction) is 20×20. Periodic boundary conditions are employed parallel to the substrate. We use 900 polymer chains in both the ordinary and deposited films, resulting in a film that is ≈22 monomers thick, where the thickness has a weak Arrhenius temperature dependence, as described in Ref. 78.

To prepare the reference ordinary film, we generate 900 polymer chains confined between repulsive walls in the *z*-direction. Our simulations are performed at high temperature ($T = 2.0$) to randomize the chain configurations, and we then cool to $T = 1.0$, where relaxation times are on the order of one time unit, so that the film readily equilibrates. We combine this film with the previously prepared substrate and remove the top repulsive interface to obtain a supported film which we equilibrate at $T = 1.0$. This film is used as the basis for subsequent cooling and re-heating runs, as well as dynamical calculations at various fixed T. The ordinary polymer film is cooled from $T = 1.0$ to 0.01 over an interval of 1.2×10^6 LJ units, using the same duration which we will use for deposition. We then reheat the sample back to $T = 1.0$ at a much higher rate 10^{-5} to provide a reference potential energy and density for the OG on heating, as shown in Fig. 1. At this heating rate, the glass transforms to an equilibrium fluid near $T = 0.40$. For simulation studies, the non-ergodicity crossover is typically near the equilibrium characteristic temperature T_c, since the inverse relaxation time at T_c roughly coincides with the cooling/heating rate manageable in simulation studies. T_c is usually associated with the mode-coupling theory,[79] although this scaling also arises in the generalized entropy theory of glass-formation.[80] The relaxation time at this computational glass transition is about 8 to 10 orders of magnitude shorter than the relaxation time at T_g defined by standard experimental methods. To study the dynamics of the ordinary film, we take configurations from

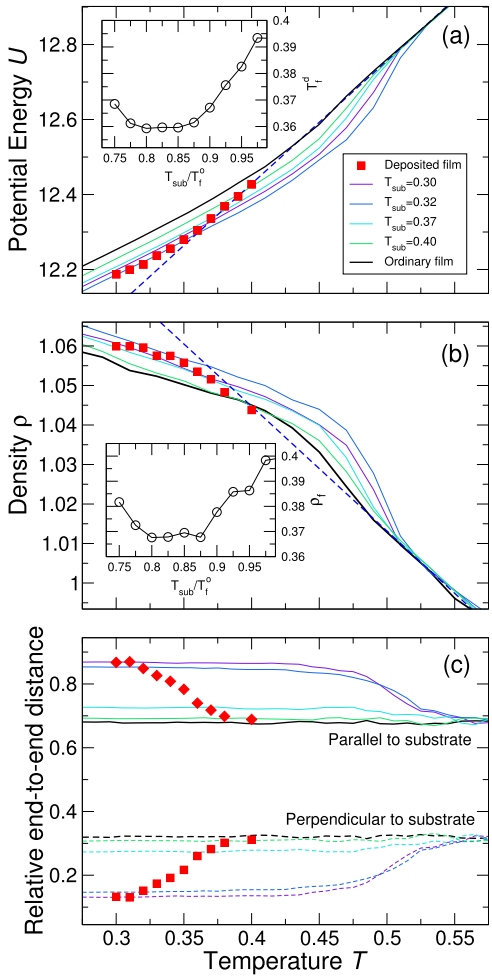

FIG. 1. (a) Potential energy of the vapor-deposited ultrastable polymer films and ordinary films during heating. The inset shows fictive temperature as a function of the substrate temperature $T_{\rm sub}$. Red squares are potential energy of the as-deposited films as a function of substrate temperature $T_{\rm sub}$ normalized by the fictive temperature of the OG film $T_f^o = 0.4$. (b) The density of the deposited film and ordinary film as a function of temperature. Red squares are the deposited film density as a function of substrate temperature. Inset shows the fictive density as a function of $T_{\rm sub}/T_f^o$. (c) Relative end-to-end distance parallel and perpendicular to the substrate of deposited and ordinary films during heating. The symbols are for the as-deposited films. The highly extended non-equilibrium state of the vapor-deposited glassy material persists until the film is heated to $T_{\rm onset}$, above which it returns to the equilibrium behavior.

the reheating run and then extend the simulations at various fixed T. For $T \gtrsim 0.40$, the polymer film is in equilibrium. Well below $T = 0.40$, the film is an out-of-equilibrium glass, but the time scale of aging is much larger than that accessible in our simulations, so that potential energy remains nearly constant in the glass. At temperatures moderately below $T = 0.40$, the film thermodynamics exhibit aging on our simulation time scale.

Inspired by the approach of Refs. 53 and 67, we model vapor-deposited films by employing the following procedure:

1. We select a chain from a supported ordinary film that was previously equilibrated at $T = 1.0$.
2. At a distance of 10 σ above the free surface, the selected chain is assigned a center-of-mass velocity $v = 0.2$ in the

direction of the substrate and propagates for 114 time units.

3. The system is allowed to relax for 600 time units. No thermostat is applied to the newly deposited chain, but the substrate and any previously deposited chains are coupled to a thermostat with substrate temperature T_{sub}.
4. The entire system is then relaxed for an additional 600 time units with all chains linked to a thermostat at temperature T_{sub}.

This process is repeated until all the 900 polymer chains have been deposited, yielding a total deposition time of $t = 1.18 \times 10^6$, the same interval used to cool ordinary GF films. We studied vapor-deposited glasses at temperatures $T = 0.30$, 0.31, 0.32, 0.33, 0.34, 0.35, 0.36, 0.37, 0.38, 0.40. The length of the isothermal trajectories to collect dynamic properties is 4.4×10^6 LJ time units. After obtaining the deposited film sample at temperature T_{sub}, we cool the sample down to $T = 0.01$ and reheat to $T = 1.0$ at the rate of 10^{-5} (the same heating rate as the ordinary film), as shown in Fig. 1. The temperature is controlled using the Nose-Hoover algorithm. The equations of motion are integrated using the rRESPA method with 3 bonded interaction updates for each non-bonded interaction update. The innermost time step is 0.002. All simulations were carried out using LAMMPS.[81]

During deposition, the chain conformation changes substantially. Specifically, the configuration for chains at the start of deposition is taken from chain configurations in an ordinary film, where chains are elongated and isotropic. As a chain approaches the substrate during deposition, the chain collapses in the vacuum. Figure 2 shows the average relative end-to-end distance $R_\perp^2/R_e^2$ and $R_\parallel^2/R_e^2$ (defined in Sec. III) of chains during the deposition, where it is apparent that chains are coiled as they approach the substrate. Once the polymer is in contact with the substrate, it is energetically favorable for the chain to again elongate (Fig. 2). The deposition process particularly favors elongation in the direction parallel to the substrate.

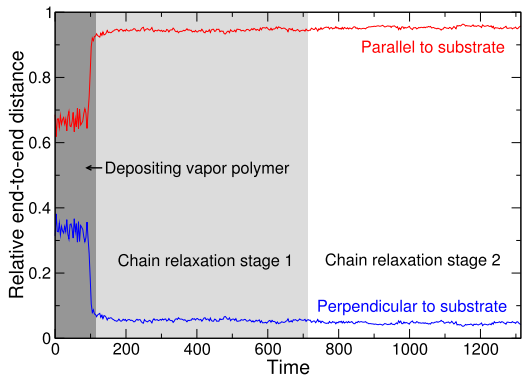

FIG. 2. Average relative end-to-end distance $R_\perp^2/R_e^2$ and $R_\parallel^2/R_e^2$ of a chain during deposition. Chains collapse in the vacuum as they approach the substrate. R_e increases parallel to the substrate once the chain contacts the surface, as shown between the dark grey and grey regions. The data are averaged over 245 polymers.

III. THERMODYNAMICS AND FILM STRUCTURE

We first establish that our vapor-deposited films exhibit the reported thermodynamic characteristics of previously studied USG films. To do so, we examine the potential energy, density, and structure of the deposited films which have been cooled to near $T = 0$ and then heated at a fixed rate of 10^{-5}. Figures 1(a) and 1(b) show a comparison of the potential energy U and density ρ for both the OG and the deposited glasses for a range of deposition (substrate) temperatures. For each glass, we can define an onset temperature T_{onset} for the transformation from glass to fluid-like behavior; for the OG, this "kink" is usually associated with (heating-rate dependent) T_g. The data clearly show that, relative to the OG, all vapor deposited glasses have a lower potential energy, have a higher density, and transform to a fluid state at a higher T_{onset}. Thus, the deposited films have the characteristics observed previously in small molecule USGs. In contrast, the experimental vapor deposition of polymer films by Priestley *et al.*[59] resulted in films with lower density than their OG counterparts. This is thought to be a consequence of the MAPLE deposition procedure, as discussed in their original work. In contrast, our deposition method for forming ultrastable glasses is intended to mimic the method of vapor deposition used for small molecules—namely, the deposition of single polymer molecules rather than polymer "globules" as in the MAPLE procedure. Thus, it is natural to expect that our deposited films should exhibit an increased density, similar to small molecule vapor-deposited glasses, rather than a decreased density.

A common interpretation of these results is that the USGs more readily reach low-energy states because of the high interfacial mobility in the USG film during the deposition process.[23–25,29,36,58] One way to characterize the stability of the deposited film is through the fictive temperature T_f. Operationally, T_f is commonly defined by the intersection of the low T behavior of U (or ρ) with a simple linear extrapolation of the corresponding high T equilibrium behavior. Since the energy and density of the deposited film depend on the substrate temperature, we can expect T_f also to vary. The insets of Figs.1(a) and 1(b) show the apparent fictive temperature relative to the fictive temperature of the OG, T_f^o. As in the experiments, this temperature ratio exhibits a minimum as a function of deposition temperature—indicating an "optimal" substrate temperature that balances the drive to low-energy states with the available time to sample low-energy configurations on the surface.[23] Our deposited films show nearly the same optimal relative temperature as experiments—around 80% to 85% of T_f^o. This behavior has also been observed in simulated small molecule and polymer deposited glasses by de Pablo and coworkers.[65,67] The similarity between the simulations and experiments is remarkable given the vastly different relaxation time scales of the simulated glasses and the experimental measurements at their respective fictive temperatures. (The ratio of the relaxation times at the respective fictive temperatures of the computational and experimental systems is on the order of 10^{10}.) Since we have established that our vapor-deposited polymer films exhibit the primary characteristics of previously studied USG films, we use the terms USG

and deposited film interchangeably in the remainder of the manuscript.

To more quantitatively relate the deposited film to the ordinary glass, we can estimate the cooling rate that an ordinary glass would have needed to obtain the same energy as that of the deposited film. To do so, we have conducted further cooling/reheating simulations of ordinary glasses at rates from $r = 3 \times 10^{-6}$ up to 10^{-3}. The difference between the potential energy of the ordinary and deposited film $\Delta U(r, T_{\rm sub}) = U_{OG}(r) - U_{USG}(T_{\rm sub})$ for a given cooling rate is essentially independent of temperature in the glassy state. In Fig. 3(a), we show $\Delta U(r)$ for the USG deposited over a range of substrate temperatures $T_{\rm sub}$. Since the data show that ΔU depends (approximately) linearly on $\ln r$, we can extrapolate at what rate $\Delta U \to 0$. In other words, we evaluate the rate that would be needed to reach the energy of the USG by ordinary cooling. We refer to this as the "fictive cooling rate" r_f of the deposited glass. In Fig. 3(b), we show the fictive cooling rate r_f as a function of $T_{\rm sub}$, which has qualitatively the same behavior as the fictive temperature as a function of $T_{\rm sub}$, namely, a minimum at $T \approx 0.32$. Compared with the ordinary film shown in Fig. 1 (and analyzed as the reference in the rest of the manuscript), r_f is from one to three orders of magnitude slower. This fictive rate also provides an expectation for the accessible increase in relaxation time, compared to the ordinary glass. Specifically, a fictive rate 3 orders of magnitude slower than the ordinary glass should mean that the deposited glass could potentially reach relaxation times roughly 3 orders of magnitude larger than that of the ordinary glass at the same temperature.

Before we characterize the dynamics of films, we consider the structure of the ordinary and deposited glasses. Metrics for the monomer-level structure, such as the pair distribution

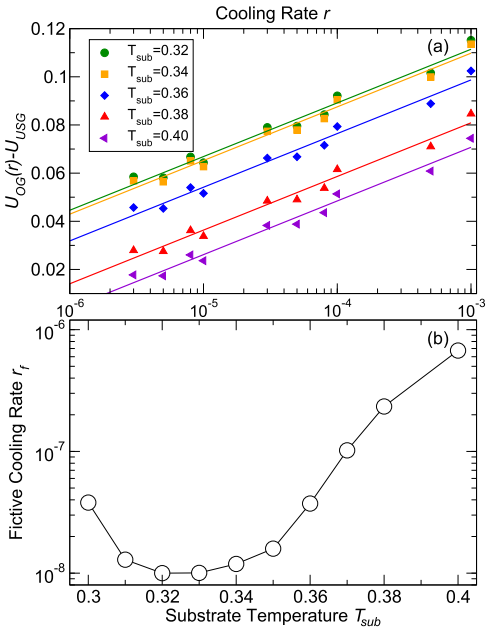

FIG. 3. (a) The difference between the potential energy of ordinary and deposited films in the glassy state $\Delta U = U_{OG}(r) - U_{USG}$ as a function of the cooling rate r. (b) By extrapolating $\Delta U \to 0$, we estimate the fictive cooling rate r_f as a function of the substrate temperature. Similar to the behavior of the fictive temperature of the deposited glasses (Figs. 1(a) and 1(b) inset), the fictive cooling rate has a minimum at ≈ 0.32.

function $g(r)$, show no obvious differences (see Fig. S1 of the supplementary material). This is not surprising since the structure of a glass changes only slightly over the same temperature range where relaxation time changes by 14 orders of magnitude. However, structural differences are apparent if we focus on chain ordering at scales larger than the chain segments. The chain orientation in the OG film is isotropic, on average. To quantify this, we calculate the parallel ($R^2_{\parallel}$) and perpendicular ($R^2_{\perp}$) components of mean-square end-to-end distance of chains, normalized by the total end-to-end distance(R^2_e). If the chains in the polymer melt exhibit random walk statistics, then $R^2_{\parallel}/R^2_e = 2/3$ and $R^2_{\perp}/R^2_e = 1/3$. Figure 1(c) confirms that the polymers are nearly isotropic in the OG, on average, for all T; changes from isotropic behavior typically only arise when the films have a thickness comparable to the monomer dimensions,[82] apart from the immediate interfacial region near the solid substrate where chains must orient with respect to the surface.[78] For all the deposited glasses, Fig. 1(c) shows that, on average, chains exhibit greatly extended dimensions in the plane of the film ($R^2_{\parallel} > 2R^2_{\perp}$), similar to the findings of Ref. 67. The overall end-to-end distance of chains in the deposited film is no more than 5% larger than the ordinary glass, so the anisotropy is primarily due to chain orientation, rather than the alteration of the chain dimensions. This behavior is analogous to isolated polymers strongly adsorbed onto asubstrate.[83] The adsorption of polymers onto highly attractive surfaces has often been observed to trap the polymers into non-equilibrium flattened configurations,[60] and this situation occurs in the multilayer deposition of polyelectrolyte films from the solution.[61–63] A similar situation arises in our vapor-deposited USG materials, where newly deposited chains adopt a highly anisotropic orientation from which it is difficult to escape. This anisotropy can relax in the case of very short chains.[67] Apparently, the high interfacial mobility allows the chains to reach a lower potential energy on the landscape by orienting in layers. On heating, the deposited polymers recover their random coil characteristics when the USG transforms back into a fluid near the onset temperature, $T_{\rm onset}$.

It is worth nothing that the experiments by Priestley and coworkers[59] did not find the anisotropy of the vapor-deposited polymer glass. However, as Ref. 59 discussed and noted above, the MAPLE deposition procedure allows polymers to form an isotropic "globule" during the deposition process, which likely prevents the anisotropy of the deposited film. In contrast, for the single molecule deposition approach we use, the significant anisotropy of chains naturally arises due to orientation with the substrate. The anisotropy of deposited glasses has also been reported in some small molecule systems. Dawson *et al.*[31] used wide-angle scattering to reveal anisotropy through the alignment of indomethacin molecules on the nm scale. In principle, the chain anisotropy of our simulations should also be reflected in a scattering profile but only at small wave vectors corresponding to the chain scale.

While the energy and density of the USG are consistent with lower energy states of the OG, we next consider if the basin shape of the minimum energy configuration, or inherent structure, is also consistent between the OG and USG. To do so, we evaluate the normal modes. We use the conjugate gradient

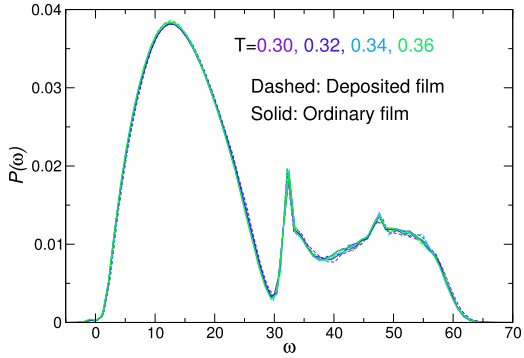

FIG. 4. The density of normal modes $P(\omega)$ obtained from the Hessian eigenvalue spectrum for both the deposited and ordinary films; $P(\omega)$ is essentially identical for all systems, indicating that the basins sampled in both the OG and USG have the same shape near the minimum.

algorithm to minimize the potential energy of the OG and USG. The normal modes ω are evaluated from the eigenvalues $m\omega^2$ of the Hessian matrix,

$$H_{i\alpha,j\beta} = \frac{\partial^2 V}{\partial r_{i\alpha}\partial r_{j\beta}}, \tag{1}$$

where i and j are particle indices and α and β are indices for spatial directions. Figure 4 shows that the density of states $P(\omega)$ for both the deposited films and OGs is essentially identical. In other words, the shape of the local potential energy basins of deposited films is indistinguishable from that of OGs. We note that the eigenmodes of the Hessian matrices are only weakly sensitive to the temperature. The density of states resembles simple Lennard-Jones fluids for $\omega < 30$;[84] higher frequencies are associated with bond vibrations. The similarity in the basin shape suggests that the USG explores basins consistent with those of the OG, supporting a close relationship between the OG and USG.

IV. STRUCTURAL RELAXATION OF THE VAPOR-DEPOSITED FILM

We next examine the structural relaxation of the deposited film and the ordinary film and contrast the difference in the relaxation time for the system as a whole versus the middle part of the film. As noted above, we separately analyze the middle part of the film since it has thermodynamic and dynamic quantities that are nearly invariant with respect to the film depth, thereby eliminating effects of the mobility gradient. We then calculate the self-part of the intermediate scattering function to determine the relaxation time in different regions of the film,

$$F_s(q,t) = \frac{1}{N}\left\langle \sum_{j=1}^{N} \exp[i\boldsymbol{q}\cdot(\boldsymbol{r}_j(t) - \boldsymbol{r}_j(0))] \right\rangle \tag{2}$$

at wave vector $\boldsymbol{q}$, where $\boldsymbol{r}_j(t)$ is the position of particle j at time t. Following standard practice, we evaluate $F_s(q,t)$ at the wave vector q_0 corresponding to the nearest neighbor periodicity. This choice provides a good correspondence with other measurements of the segmental relaxation time. We evaluate $F_s(q_0,t)$ for the whole film and $F_s^{\mathrm{mid}}(q_0,t)$ for the middle, where the middle part of the film is defined by the region within $\pm 5\sigma$ relative to the center of mass of the film in the direction perpendicular to the substrate. We average $F_s(q_0,t)$ over time

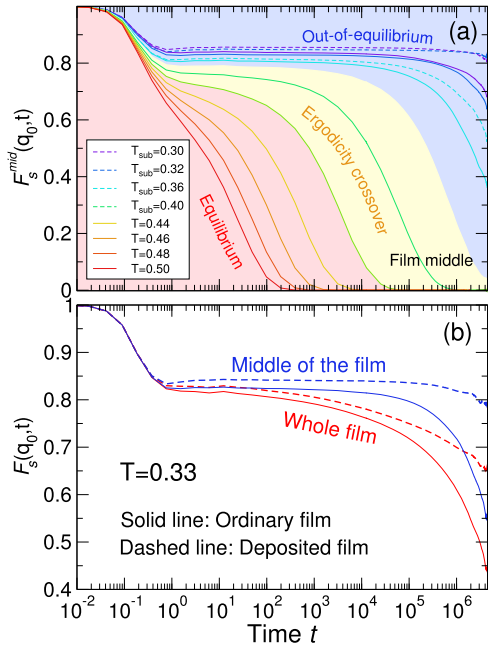

FIG. 5. The self-intermediate scattering function for (a) the middle of the ordinary and deposited films and (b) comparison between the middle of the film and the film as a whole. Solid curves represent ordinary films and dashed curves represent deposited films. The background color provides an indication of the crossover from equilibrium to glassy states. The film as a whole relaxes faster than the middle region of the film at a large time due to the free interface. For the purposes of clarity in panel (b), $F_s(q_0,t)$ at other temperatures is not shown. The middle of the film is defined by the region within $\pm 5\sigma$ from the center of mass of the film in the direction perpendicular to the substrate.

origins for a single sample of the film. We have also calculated $F_s(q_0,t)$ without averaging over time origins (Fig. S2 of the supplementary material), which shows that the time averaging does not qualitatively change the behavior $F_s(q_0,t)$. Figure 5 shows the behavior of $F_s(q_0,t)$ and $F_s^{\mathrm{mid}}(q_0,t)$ for both the ordinary and deposited films for a range of temperatures. As expected, the deposited films show slower relaxation than the ordinary film, an effect which is more pronounced in the middle of the film. Specifically, $F_s^{\mathrm{mid}}(q_0,t)$ in both the ordinary and deposited films exhibits an appreciably longer plateau region than the overall film dynamics, and thus a longer α-relaxation time.

We define the structural relaxation time τ by fitting the primary decay of $F_s(q_0,t)$ with a stretched exponential,

$$F_s(q_0,t) = A\exp[-(t/\tau)^{\beta}]. \tag{3}$$

For $T \lesssim 0.40$, $F_s(q_0,t)$ does not fully decay to zero on the time scale of our simulations. Since τ at these low T relies on an extrapolation of the fit to the stretched-exponential form, we only report τ data for films for which $F_s(q_0,t)$ relaxes to at least 80% of the plateau value of $F_s(q_0,t)$. The resulting τ values are shown in Figs. 6 and 7; for non-equilibrium states, the reported τ should be considered a lower bound, since further aging is expected to increase the relaxation time of the film. Figure 6 shows that the relaxation time of the deposited glass is larger than that of an OG below $T = 0.38$ for the middle of the film, consistent with previous studies. That said, τ of the USG film in the glass state falls short of the relaxation time that would be expected by extrapolating the Vogel-Fulcher-Tammann (VFT) fit to the equilibrium data;

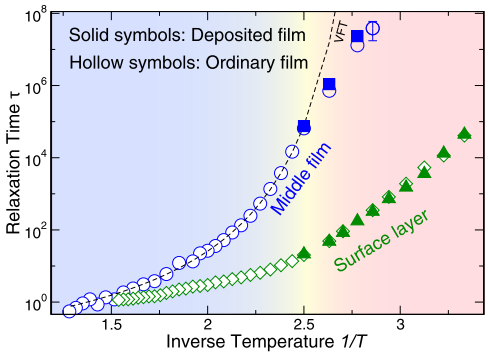

FIG. 6. The relaxation time τ of $F_s(q_0, t)$ of the ordinary and vapor-deposited films as a function of temperature for the middle region and surface region of the films. Blue symbols represent the relaxation time τ in the middle of the film and the green symbols represent τ at the surface layer. The background color provides an indication of the crossover from equilibrium to glassy states. We only indicate the uncertainty if the size of the error bar exceeds the size of the symbol. We evaluate τ from the stretched exponential fit (Eq. (3)).

additionally, τ is not as large as might be expected from the effective cooling rate (Fig. 3), which is based on the changes in the energy of the deposited film. For $T < 0.36$, it is apparent from $F_s(q_0, t)$ that τ is larger for the deposited films, but we are unable to quantitatively estimate τ at those temperatures since $F_s(q_0, t)$ does not decay significantly. However, based on the fictive cooling rates in Fig. 3, we would expect relaxation time in the deposited glass at these T to be 2 to 3 orders of magnitude larger than that of the ordinary glass. It is notable that our simulated films become glassy at a much higher temperature than they would if we could cool at rates comparable to experiments; a similar density change at the experimental T_g would result in a larger change in the relaxation time than observed at our computational cooling rates. The dynamics are nearly identical in OGs and USGs near the free surface, as the enhanced mobility near the free interface allows both types of films to readily equilibrate to similar states.

To better characterize the difference between the interfacial relaxations in the interior of the film, we consider the gradient of relaxation times across the film profile of both the polymer USG and OG films. Figure 7 shows $\tau(z, T)$ for layers of thickness 0.875 parallel to the substrate; the layer thickness corresponds to the period of the oscillation of the monomer

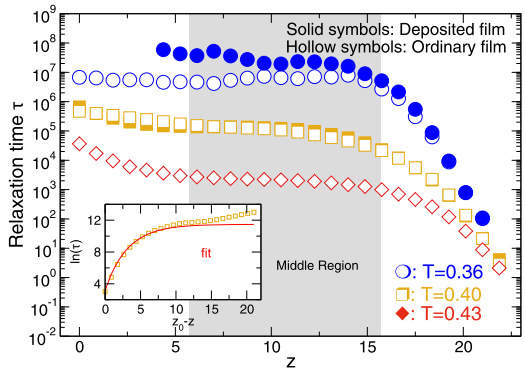

FIG. 7. Relaxation time τ as a function of distance from the film substrate. τ is obtained from Eq. (3). The inset shows the fit to the distance dependence of τ from the free interface using Eq. (4), which defines an interfacial scale for the relaxation gradient; z_0 is the position of the free surface interface defined by a density cutoff 0.1.

density profile along the z-direction. We again see that $\tau(z)$ near the surface is significantly enhanced relative to the film interior and that the relaxation time of the interior of the USG is somewhat larger than that of the OG. The τ difference is not as large as one might be anticipated given the differences in energy and density between the OG and USG.

We next define a scale for the interfacial gradient in the relaxation time. Following earlier works,[70,78,85] we define the length scale ξ of the enhanced dynamics using the relation,

$$\ln(\tau(z)) = \ln(\tau_{\text{mid}}) \left[1 - C \exp\left[\frac{-|z - z_0|}{\xi}\right]\right], \qquad (4)$$

where C describes the amplitude of deviations from τ_{mid} and z_0 is the location of the interface. This length scale ξ characterizes the thickness of the mobile layer in the film (Fig. 8). As expected from previous studies,[70,71,78,86] ξ increases on cooling in the equilibrium region $T > T_g$. This equilibrium growth has been associated with the scale of cooperative motion.[70,71] Somewhat surprisingly, this trend in ξ reverses upon entering the non-equilibrium glassy regime, i.e., ξ starts to increase on heating, similar to a crystal upon approaching its melting point.[87] This inverted trend of the interfacial mobile layer with T is consistent with experimental measurements of the mobile layer thickness in polystyrene thin films in the glass state using a photobleaching technique.[72] The deposited films generally have a somewhat larger ξ than that of OGs.

We can gain insight into the reversal in the interfacial scale ξ with T by considering the mismatch of the relaxation in the film interior relative to that of the interfacial relaxation, $\tau_{\text{mid}}/\tau_{\text{surface}}$. Figure 8(b) shows that this ratio grows rapidly on cooling in the equilibrium regime, but the trend reverses in

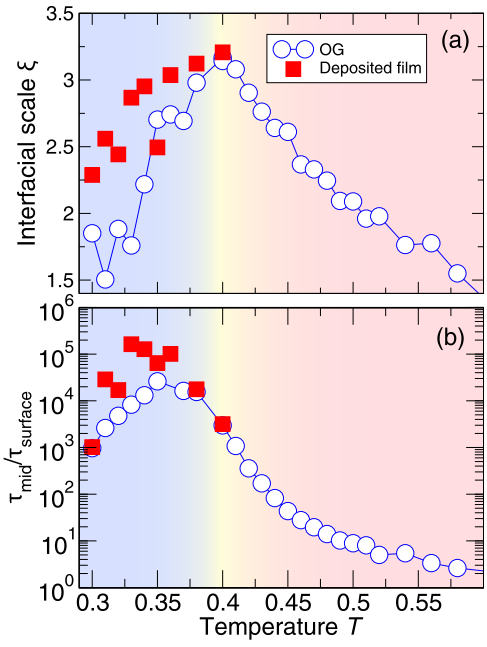

FIG. 8. Interfacial scale ξ of both the OG and USG as a function of temperature. The interfacial scale is non-monotonic: ξ grows on cooling in the equilibrium regime, but in non-equilibrium states ξ grows on heating, consistent with experiments.[72] (b) The ratio of the interior to surface relaxation time $\tau_{\text{mid}}/\tau_{\text{surface}}$. The narrowing gap between relaxations in the middle and interfacial regions in the non-equilibrium state is partially responsible for the drop of ξ in the glass. The background color provides an indication of the crossover from equilibrium to glassy states.

the glassy regime. Evidently, the (non-equilibrium) relaxation time in the film center has a relatively weak T-dependence in the glassy state, while the free surface of the film remains in equilibrium with a substantial T dependence. $\tau_{\rm mid}/\tau_{\rm surface}$ reaches a maximum ratio of $\approx 10^5$. If we assume that the equilibrium $\tau_{\rm mid}$ and $\tau_{\rm surface}$ follow a VFT form, this difference in relaxation between the film interior and interface is predicted to be even larger near the experimental T_g; specifically, we estimate that a mobility ratio $\tau_{\rm mid}/\tau_{\rm surface}$ could be as large as 10^{11} near the experimental T_g. Experimental estimates of this ratio show that it can indeed be quite large, with surface relaxation being enhanced by a factor as large as 10^7.[88–91]

V. CHARACTERIZATION OF SPATIAL AND TEMPORAL HETEROGENEOUS DYNAMICS

It is well known that below an onset temperature T_A, the dynamics of GF fluids can be separated into groups with distinct spatial and temporal scales, a phenomenon called dynamical heterogeneity. In this section, we characterize the extent of dynamical heterogeneity in the deposited film and contrast it with the OG. In the film system, the mobility gradient, which is characterized by enhanced interfacial dynamics and suppressed dynamics near the substrate, represents a "fixed" heterogeneity that can interfere with common metrics to quantify the local dynamical heterogeneity. To distinguish these two contributions to heterogeneity, we study the heterogeneous dynamics of the film in the interfacial and bulk-like middle region separately, considering both the monomer displacement and string-like cooperative motion.

One of the basic ways to quantify heterogeneous dynamics is to measure the degree to which the motion of the particles deviates from Gaussian behavior, using a non-Gaussian parameter,

$$\alpha_2(t) = \frac{3}{5}\frac{\langle \Delta \boldsymbol{r}^4(t)\rangle}{\langle \Delta \boldsymbol{r}^2(t)\rangle^2} - 1, \tag{5}$$

where $\langle \Delta \boldsymbol{r}^2(t)\rangle$ is the mean-square displacement of the monomers. $\alpha_2(t)$ commonly features a peak, the amplitude $\alpha_2^{\rm max}$ of which indicates the degree of spatial heterogeneity, as well as a characteristic time scale t^* of spatial heterogeneous dynamics. Both t^* and $\alpha_2^{\rm max}$ grow as the temperature decreases, a result of the increasing degree of spatially correlated motion.[92,93] We evaluate $\alpha_2(t)$ (Fig. 9) for both OGs and USGs, for the film as a whole and the middle of the film (defined in Sec. IV). In the non-equilibrium region, both the characteristic time scale and amplitude of α_2 for the middle of deposited films are larger than those of OGs (Fig. 9(a)). This deviation becomes more pronounced as the temperature decreases. In fact, at $T \le 0.33$, the peak of $\alpha_2^{\rm mid}$ of the deposited film is shifted to such a large time scale that it is out of the range accessible by our simulations, while for the OG, the peak is still apparent.

We next contrast the heterogeneous dynamics in the middle of the film with that of the overall film to assess the effects of the mobility gradient on the dynamical heterogeneity. As mentioned, α_2 has two major contributions: the local heterogeneous dynamics and the macroscopic mobility gradient. In Fig. 9(b), we show that α_2 of the whole film is much larger than that of the middle of the film. This is due to the mobility

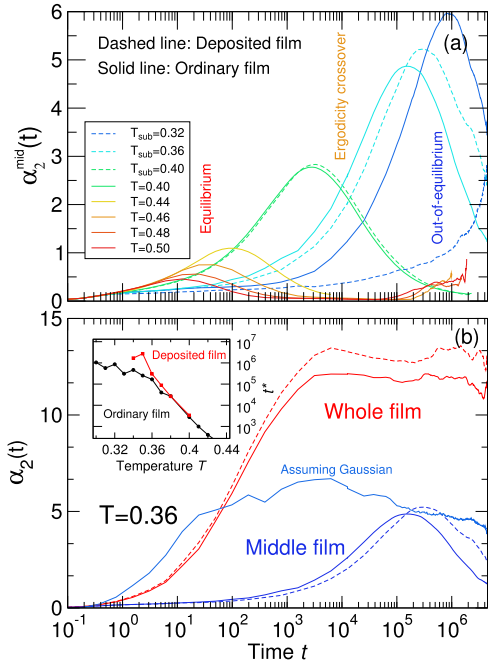

FIG. 9. The non-Gaussian parameter α_2 for (a) the middle of the film for many T and (b) comparison between the middle ($\alpha_2^{\rm mid}$) and whole film (α_2). The curves are color-coded from high temperature (red) to low temperature (purple). Panel (a) shows a significant increase in the scale and magnitude of α_2 at low T. Panel (b) shows that the whole film has much larger α_2 than that of the middle of the film. This difference is largely due to the static mobility gradient across the film. Panel (b) also shows the effect of the mobility gradient on α_2, if we assume that the displacements within horizontal layers are perfectly Gaussian while imposing a gradient on the mean displacement (light blue curve).

gradient within the film, which itself is a form of dynamical heterogeneity. This gradient makes a substantial contribution to the film relaxation for $T \lesssim 0.42$, becoming the predominant dominant contribution in the glass state. To better illustrate this point, we model the contribution of the mobility gradient to α_2 using the approximation that the monomer dynamics at a fixed film depth strictly obey a Gaussian distribution. To do so, we first calculate the mean-square displacement $\langle \Delta \boldsymbol{r}^2(t)\rangle$ of the monomer layers parallel to the substrate. Assuming Gaussian behavior within the layer, $\langle \Delta \boldsymbol{r}^4(t)\rangle = \frac{5}{3}\langle \Delta \boldsymbol{r}^2(t)\rangle^2$, and thus the contribution from a gradient with purely Gaussian displacements equals

$$\tilde{\alpha}_2(t) = N_{\rm layer}\frac{\sum_n^{N_{\rm layer}} \left\langle \Delta \boldsymbol{r}^2(t)\right\rangle_n^2}{\left(\sum_n^{N_{\rm layer}} \langle \Delta \boldsymbol{r}^2(t)\rangle_n\right)^2} - 1, \tag{6}$$

where $N_{\rm layer}$ is the number of layers. The light blue, in Fig. 9(b), curve shows that a gradient of the mobility with locally Gaussian dynamics results in a contribution to α_2 that is larger than α_2 in the middle of the film. In particular, this $\tilde{\alpha}_2$ estimate exhibits a very broad peak due to the persistence of the gradient, unlike α_2 in the middle of the film. This is precisely why α_2 for the whole film does not asymptote to zero in the scale of our simulation. In short, the dynamical heterogeneity measured by α_2 for the film as a whole is greatly influenced by the mobility gradient.

The difference in α_2 between the OG and USG is more easily captured by the T-dependence of $\alpha_2^{\rm max}$ and t^* (Fig. 10).

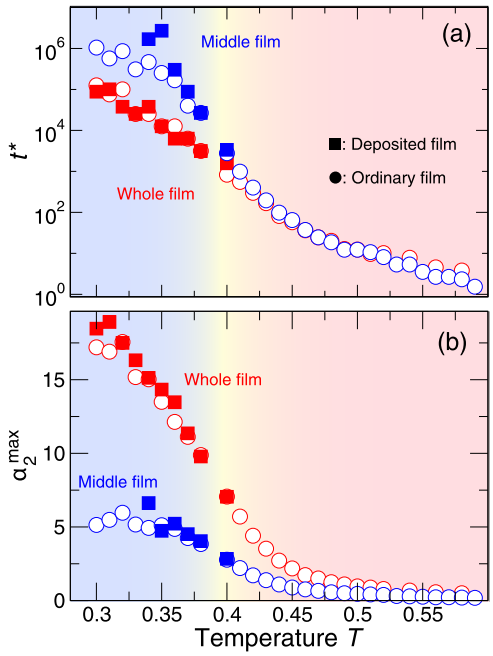

FIG. 10. (a) The time scale t^* and (b) amplitude $\alpha_2^{\max}$ of the non-Gaussian parameter for both the deposited and ordinary films as a function of temperature. In order to distinguish the contribution of the mobility gradient to α_2 from that of the intrinsic dynamical heterogeneity, we separately show the behavior of the middle of the film and the film as a whole. The background color provides an indication of the crossover from equilibrium to glassy states.

We observe that the time scale t^* for the deposited film and the ordinary film is *similar* for the film as a whole (shown as red curves in Fig. 10(a)), due to the similar mobility gradient in both systems that dominates α_2. However, $t^*_{\rm mid}$ of the deposited film deviates from that of the OG for $T \lesssim 0.38$, an indication of increased heterogeneous dynamics. In Fig. 10(b), $\alpha_2^{\max}$ of the whole film is slightly larger than that of the OG. This mainly stems from the increased extent and time scale of heterogeneous dynamics in the middle of the film.

VI. STRING-LIKE COOPERATIVE REARRANGEMENTS IN THE USG AND OG FILMS

It has been established that one manifestation of dynamical heterogeneity in GF liquids is cooperative rearrangement, a key ingredient to the theory developed by Adams and Gibbs (AG).[16] According to the AG theory, relaxation in GF liquids is an activated process, and the height of the activation barrier is proportional to the size of hypothetical cooperatively rearranging regions (CRRs), but AG provided no well-defined prescription for defining CRRs. The AG theory has motivated many theoretical and simulation studies to examine and define the cooperative nature of the rearrangements. In particular, string-like cooperative motions, first described by Donati *et al.*,[94] have emerged as a candidate to quantify the CRRs, and it has been shown that the size of string-like motions follows the growth of the relaxation barrier.[95–98] In polymer films, it has also been argued that this CRR scale tracks the scale of the interfacial region.[70,71]

Motivated by these facts, we now examine the cooperative nature of monomer rearrangements in the USG and OG films using the average string size. Following procedures developed in earlier works,[94,95,99] we quantify string-like rearrangements in these GF materials. Conceptually, the monomers are identified as elements of a string if they replace a neighboring monomer over a time interval t, independent of whether the two monomers are in the same chain. The cluster of such replacing monomers determines the string size L. Like $\alpha_2(t)$, $\langle L(t)\rangle$ has a peak at an intermediate time scale characterized by its peak time t_L and amplitude L (Fig. 11(a)). The time scale t_L and amplitude L of the peak grow larger upon cooling, indicating the increasing degree of cooperative motions and dynamical heterogeneity. We have also considered polymer-specific effects on the string-like correlated motion. Specifically, Aichele *et al.*[100] have shown that, in the bulk polymer system, the string-like cooperative motion is not strongly correlated with chain connectivity so that the collective motion does not take a repetitive form on the timescales of segmental relaxation. To confirm this expected behavior in the USG materials, we follow the same procedure as in the work of Aichele *et al.*, and Fig. S5 of the supplementary material shows the average string size formed by contiguous chain segments $L_{\rm seg}(t)$. As found in the earlier work for the bulk system, there is a substantial contribution from interchain monomer displacements to string-like motion.

We now contrast the behavior of string-like displacements in the OG and USG. Figure 11(a) shows the average string length in the middle of the film as a function of time for the USGs and OGs for many T. For $T \lesssim 0.36$, the characteristic time t_L of the middle of the USG film is significantly longer than that of the OG at the same temperature. This trend is more clearly shown in Fig. 12(a) where t_L is plotted directly. For $T \lesssim 0.35$, t_L for the USG is beyond the accessible range of our simulations, while that of the OG is still accessible. Similar

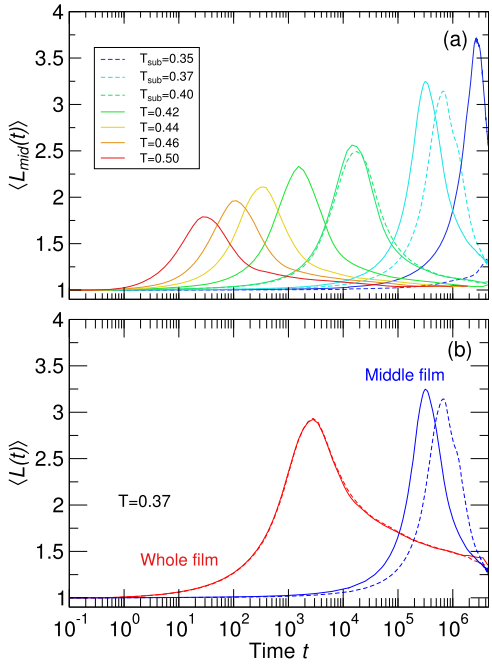

FIG. 11. Average string length $\langle L(t)\rangle$ in (a) the middle of the film for many T and (b) the comparison between the whole film and middle of the film for both the deposited and ordinary films at $T = 0.37$. The dashed curves indicate deposited films. We use color ranging from red, yellow, green, blue, to purple to represent the range of temperatures from high to low.

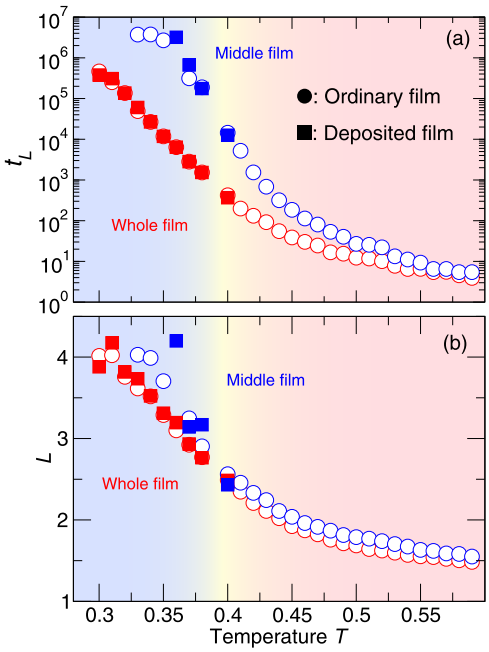

FIG. 12. (a) The characteristic time scale t_L of average string size and (b) the maximum of the average string length L as a function of temperature for both the deposited and ordinary films. Circle and square symbols represent ordinary and deposited films, respectively. In order to distinguish the contribution of the mobile surface layer to L from that of the intrinsic dynamical heterogeneity, we separately show the behavior of the middle of the film and the film as a whole. The background color provides an indication of the crossover from equilibrium to glassy states.

to the behavior of t_L, we observe that the peak L of the middle of the deposited film at temperature $T \lesssim 0.36$ is similar to that of the OG in our simulations. We expect a larger value for the deposited glass at lower T based on the longer relaxation and lower energy, and the data for the lowest T are consistent with this possibility. Apparently, the dynamical heterogeneity in the middle of the deposited film is more pronounced than the OG for $T \lesssim 0.36$.

The relative behavior of string-like motion becomes apparent if we consider the film as a whole. To illustrate how the enhanced surface dynamics of the film can affect $L(t)$, we directly contrast $L(t)$ of the whole film with that of the middle of the film (Fig. 11(b)). We observe a significant shift in the time scale t_L for the middle of the film in comparison to the film as a whole for both the OG and USG. The peak L is slightly larger in the middle of the film than for the film as a whole for both the OG and USG (Fig. 12(b)), indicating that the intrinsic dynamical heterogeneity in the middle of the film has a larger extent than that of the film as a whole. This is a result of the fact that the mobile monomers for the overall film are concentrated in the mobile surface layer, and therefore the rearrangements near the surface dominate the extent of cooperative motion. As a consequence, the amplitude L and the characteristic time t_L for the film as a whole are nearly *identical* for the USG and OG (Figs. 11(b) and 12 (red curves)). The similarity in t_L is consistent with the nearly *identical* relaxation time of the surface layer for the OG and USG (Fig. 6). The similar behavior of L for the OG and USG as a whole is parallel to the similarity of α_2 for these glasses. However, the origin of the similarity in α_2 for the whole film is from the mobility gradient across the entire sample (as shown in Sec. V), rather than only from the interfacial layer. This is another indication that the large mobility gradient across the film profile substantially affects estimates of dynamical heterogeneity. These results emphasize the importance of characterizing the dynamical heterogeneity of the OG and USG in the middle regions of thin polymer films of these materials.

VII. DISCUSSION AND CONCLUSION

In summary, we have used computer simulations to mimic the vapor deposition process of an unentangled polymer film. We have verified that our simulated USGs share the same thermodynamic features found experimentally for vapor-deposited, small molecule glasses. The density of our polymer USGs differs from deposited polymer glasses made by the MAPLE method,[59] owing to differences in the deposition procedure. We characterized the dynamical heterogeneity in the deposited film. For both the ordinary and ultrastable glasses, we find that the enhanced surface mobility largely affects both the scale and the magnitude of the heterogeneous motions. Specifically, the mobility gradient of the film dominates the overall non-Gaussian parameter α_2, overwhelming the contribution from the interior of the film. Consequently, α_2 for the ordinary and ultrastable glasses are only noticeably different when focusing on the dynamical behavior near the film center. The average string size of the ordinary and ultrastable glasses for the film as whole is also rather similar, but for a different reason. Specifically, mobile particles in the film are concentrated at the highly mobile interface, which has nearly identical dynamics in both the ultrastable and ordinary glasses. Again, the difference in cooperative displacements between the ultrastable and ordinary glasses becomes apparent when we focus on the middle of the film. For both α_2 and L at the middle of the film, the ultrastable glass shows a behavior consistent with the properties of a moderately aged ordinary glass, i.e., larger relaxation time, higher density, and lower enthalpy. Our findings demonstrate that common measurements of heterogeneous dynamics for the film as a whole are not sufficient to distinguish significant differences between the ordinary film and ultrastable vapor-deposited films. Instead, one must be careful to separate the dynamics in the film center.

We also characterize the thickness ξ of the mobile surface layer, which grows with the increasing degree of cooperative motions on cooling in the equilibrium regime. The T dependence of ξ reverses upon entering the non-equilibrium glassy regime, consistent with experimental measurements. We attribute this reversal in part to the diminishing ratio of interior to surface relaxation in the glass. The interfacial scale ξ of the deposited film is somewhat larger than that of the ordinary film in the glassy regime. More significantly, the reversal in the T dependence of ξ in the glass is not mirrored by the T dependence of L. Apparently, the string size and interfacial scale decouple in the non-equilibrium regime. This unexpected observation deserves further investigation.

A natural question is whether our findings are specific to the polymer system we study, or if a similar behavior can be expected in small molecule deposited glasses. To address this question, we carried out simulations of a vapor-deposited

glass described by the 80/20 binary Lennard-Jones mixture (popularized by the work of Kob and Anderson[101]) and used as the standard model for many studies of glass formation; this is the same model examined by de Pablo and collaborators in vapor deposition simulations.[53,66] Simulation details for this system are provided in the supplementary material. We find that the binary LJ system shows the same qualitative behavior as the polymeric system for the heterogeneity of the deposited glass relative to that of the ordinary glass (Fig. 13). Specifically, the measures of heterogeneity in the vapor-deposited glass indicate a larger time scale for the heterogeneous dynamics than that of the ordinary film, which is expected to also result in larger dynamical structures. Additionally, the binary LJ systems exhibit the same effect of the mobility gradient profile on the heterogeneity when examining the film as a whole, emphasizing the importance of separating interfacial effects from the film interior. These simulations suggest that vapor deposition, at least the type of vapor deposition process we consider, leads to a class of materials having qualitatively similar dynamic properties. On the other hand, we must be cognizant that vapor deposited films are inherently non-equilibrium materials whose properties depend on the nature of the deposition process, as the results of Priestley and coworkers MAPLE vapor deposited[59] films clearly demonstrate.

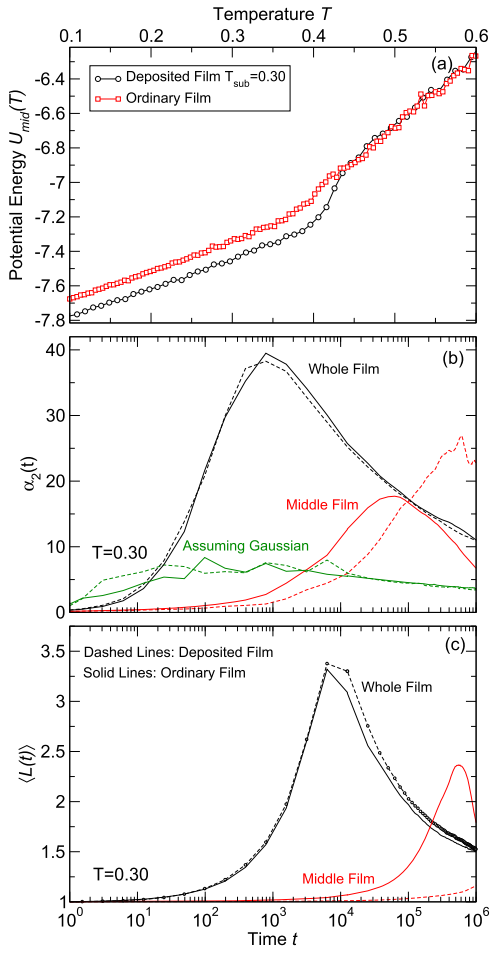

FIG. 13. (a) The potential energy in the middle of the vapor-deposited and ordinary binary mixture glass films during heating. (b) The non-Gaussian parameter α_2 of the deposited and ordinary binary mixture films. (c) The average string length $\langle L(t)\rangle$ of the deposited and ordinary binary mixture films. Panels (b) and (c) follow the same scheme as Figs. 9(b) and 11(b), respectively.

Further research is necessary in order to determine if the ultrastable vapor-deposited film can be formally considered as equivalent to an aged ordinary polymer glass. Our simulations show that the relaxation time and dynamical heterogeneity of the USG resemble the properties of a modestly aged ordinary film with a larger relaxation time, a higher density, and a larger degree of heterogeneity. Structurally, these films are different due to the orientation of deposited chains, an effect that is absent in many small molecule glasses. On the other hand, care is warranted in extrapolating the dynamic properties of ultrastable vapor-deposited films from differences in the thermodynamic properties of these materials alone.

SUPPLEMENTARY MATERIAL

See supplementary material for additional details on the film structure and dynamics, as well as simulation details for the binary Lennard-Jones mixture vapor-deposited film.

ACKNOWLEDGMENTS

Computer time was provided by Wesleyan University. This work was supported in part by NIST Award No. 70NANB15H282. We also thank J. de Pablo and J. Helfferich for valuable assistance to validate our deposited glass simulations.

[1] S. J. Holland, B. J. Tighe, and P. L. Gould, J. Controlled Release **4**, 155 (1986).
[2] M. Duclot and J. L. Souquet, J. Power Sources **97-98**, 610 (2001).
[3] C. Liu, F. Li, L.-P. Ma, and H.-M. Cheng, Adv. Mater. **22**, E28 (2010).
[4] G. W. White and S. H. Cakebread, Int. J. Food Sci. Technol. **1**, 73 (1966).
[5] C. L. E. Struik, Polymer Eng. Sci. **17**, 165 (1977).
[6] Y. H. Roos, in *Food Materials Science*, edited by J. M. Aguilera and P. J. Lillford (Springer, 2008), pp. 67–81.
[7] G. Harsányi, Sens. Rev. **20**, 98 (2000).
[8] D. W. Hutmacher, J. Biomater. Sci., Polym. Ed. **12**, 107 (2001).
[9] D. Bratton, D. Yang, J. Dai, and C. K. Ober, Polym. Adv. Technol. **17**, 94 (2006).
[10] C. A. Angell, Science **267**, 1924 (1995).
[11] R. Stevenson, D. Dingwell, S. Webb, and N. Bagdassarov, J. Volcanol. Geotherm. Res. **68**, 297 (1995).
[12] J. Aizenberg, L. Addadi, S. Weiner, and G. Lambert, Adv. Mater. **8**, 222 (1996).
[13] R. A. Baragiola, Planet. Space Sci. **51**, 953 (2003).
[14] C. A. Angell, J. Non-Cryst. Solids **354**, 4703 (2008).
[15] D. L. Anderson, Science **267**, 1618 (1995).
[16] G. Adam and J. H. Gibbs, J. Chem. Phys. **43**, 139 (1965).
[17] T. R. Kirkpatrick, D. Thirumalai, and P. G. Wolynes, Phys. Rev. A **40**, 1045 (1989).
[18] J. Dyre, N. Olsen, and T. Christensen, Phys. Rev. B **53**, 2171 (1996).
[19] P. G. Debenedetti and F. H. Stillinger, Nature **410**, 259 (2001).
[20] J. P. Bouchaud and G. Biroli, J. Chem. Phys. **121**, 7347 (2004).
[21] S. A. Kivelson and G. Tarjus, Nat. Mater. **7**, 831 (2008).
[22] J. C. Mauro, Y. Yue, A. J. Ellison, P. K. Gupta, and D. C. Allan, Proc. Natl. Acad. Sci. U. S. A. **106**, 19780 (2009).
[23] S. F. Swallen, K. L. Kearns, M. K. Mapes, Y. S. Kim, R. J. McMahon, M. D. Ediger, T. Wu, L. Yu, and S. Satija, Science **315**, 353 (2007).
[24] K. L. Kearns, S. F. Swallen, M. D. Ediger, T. Wu, and L. Yu, J. Chem. Phys. **127**, 154702 (2007).
[25] K. L. Kearns, S. F. Swallen, M. D. Ediger, T. Wu, Y. Sun, and L. Yu, J. Phys. Chem. B **112**, 4934 (2008).
[26] S. F. Swallen, K. L. Kearns, S. Satija, K. Traynor, R. J. McMahon, and M. D. Ediger, J. Chem. Phys. **128**, 214514 (2008).

[27] S. Léonard and P. Harrowell, J. Chem. Phys. **133**, 244502 (2010); e-print arXiv:1008.4438.
[28] K. L. Kearns, T. Still, G. Fytas, and M. D. Ediger, Adv. Mater. **22**, 39 (2010).
[29] K. L. Kearns, K. R. Whitaker, M. D. Ediger, H. Huth, and C. Schick, J. Chem. Phys. **133**, 14702 (2010).
[30] S. F. Swallen, K. Windsor, R. J. McMahon, M. D. Ediger, and T. E. Mates, J. Phys. Chem. B **114**, 2635 (2010).
[31] K. J. Dawson, L. Zhu, L. Yu, and M. D. Ediger, J. Phys. Chem. B **115**, 455 (2011).
[32] K. Dawson, L. Zhu, L. A. Kopff, R. J. McMahon, L. Yu, and M. D. Ediger, J. Phys. Chem. Lett. **2**, 2683 (2011).
[33] K. Dawson, L. A. Kopff, L. Zhu, R. J. McMahon, L. Yu, R. Richert, and M. D. Ediger, J. Chem. Phys. **136**, 094505 (2012).
[34] S. S. Dalal and M. D. Ediger, J. Phys. Chem. Lett. **3**, 1229 (2012).
[35] A. Sepúlveda, E. Leon-Gutierrez, M. Gonzalez-Silveira, M. T. Clavaguera-Mora, and J. Rodríguez-Viejo, J. Phys. Chem. Lett. **3**, 919 (2012).
[36] A. Sepúlveda, S. F. Swallen, L. A. Kopff, R. J. McMahon, and M. D. Ediger, J. Chem. Phys. **137**, 204508 (2012).
[37] Z. Chen, A. Sepúlveda, M. D. Ediger, and R. Richert, J. Chem. Phys. **138**, 12A519 (2013).
[38] K. R. Whitaker, D. J. Scifo, M. D. Ediger, M. Ahrenberg, and C. Schick, J. Phys. Chem. B **117**, 12724 (2013).
[39] C. Rodríguez-Tinoco, M. Gonzalez-Silveira, J. Ràfols-Ribé, A. F. Lopeandia, M. T. Clavaguera-Mora, and J. Rodriguez-Viejo, J. Phys. Chem. B **118**, 10795 (2014).
[40] T. Pérez-Castañeda, C. Rodríguez-Tinoco, J. Rodríguez-Viejo, and M. A. Ramos, Proc. Natl. Acad. Sci. U. S. A. **111**, 11275 (2014).
[41] A. Sepúlveda, M. Tylinski, A. Guiseppi-Elie, R. Richert, and M. D. Ediger, Phys. Rev. Lett. **113**, 45901 (2014).
[42] S. S. Dalal, D. M. Walters, I. Lyubimov, J. J. de Pablo, and M. D. Ediger, Proc. Natl. Acad. Sci. U. S. A. **112**, 4227 (2015).
[43] A. Gujral, K. A. O'Hara, M. F. Toney, M. L. Chabinyc, and M. Ediger, Chem. Mater. **27**, 3341 (2015).
[44] D. M. Walters, R. Richert, and M. D. Ediger, J. Chem. Phys. **142**, 134504 (2015).
[45] J. Frischeisen, D. Yokoyama, A. Endo, C. Adachi, and W. Brütting, Org. Electron. **12**, 809 (2011).
[46] D. Yokoyama, J. Mater. Chem. **21**, 19187 (2011).
[47] I. Cho, S. H. Kim, J. H. Kim, S. Park, and S. Y. Park, J. Mater. Chem. **22**, 123 (2012).
[48] C. Kim, K. L. Marshall, J. U. Wallace, and S. H. Chen, J. Mater. Chem. **18**, 5592 (2008).
[49] K. Ishii, H. Nakayama, S. Hirabayashi, and R. Moriyama, Chem. Phys. Lett. **459**, 109 (2008).
[50] K. Ishii, H. Nakayama, R. Moriyama, and Y. Yokoyama, Bull. Chem. Soc. Jpn. **82**, 1240 (2009).
[51] S. S. Dalal, A. Sepúlveda, G. K. Pribil, Z. Fakhraai, and M. D. Ediger, J. Chem. Phys. **136**, 204501 (2012).
[52] S. S. Dalal, Z. Fakhraai, and M. D. Ediger, J. Phys. Chem. B **117**, 15415 (2013).
[53] S. Singh, M. D. Ediger, and J. J. de Pablo, Nat. Mater. **12**, 139 (2013).
[54] E. León-Gutierrez, G. Garcia, M. T. Clavaguera-Mora, and J. Rodríguez-Viejo, Thermochim. Acta **492**, 51 (2009).
[55] E. Leon-Gutierrez, A. Sepúlveda, G. Garcia, M. T. Clavaguera-Mora, and J. Rodríguez-Viejo, Phys. Chem. Chem. Phys. **12**, 14693 (2010).
[56] S. L. L. M. Ramos, M. Oguni, K. Ishii, and H. Nakayama, J. Phys. Chem. B **115**, 14327 (2011).
[57] M. Ahrenberg, Y. Z. Chua, K. R. Whitaker, H. Huth, M. D. Ediger, and C. Schick, J. Chem. Phys. **138**, 24501 (2013).
[58] Z. Fakhraai, T. Still, G. Fytas, and M. D. Ediger, J. Phys. Chem. Lett. **2**, 423 (2011).
[59] Y. Guo, A. Morozov, D. Schneider, J. W. Chung, C. Zhang, M. Waldmann, N. Yao, G. Fytas, C. B. Arnold, and R. D. Priestley, Nat. Mater. **11**, 337 (2012).
[60] S. Cui, C. Liu, and X. Zhang, Nano Lett. **3**, 245 (2003).
[61] D. Kovacevic, S. Van der Burgh, A. De Keizer, and M. A. Cohen Stuart, Langmuir **18**, 5607 (2002).
[62] Q. Wang, Soft Matter **5**, 413 (2009).
[63] A. Zhuk, V. Selin, I. Zhuk, B. Belov, J. F. Ankner, and S. A. Sukhishvili, Langmuir **31**, 3889 (2015).
[64] J. Baschnagel and F. Varnik, J. Phys.: Condens. Matter **17**, R851 (2005).
[65] S. Singh and J. J. de Pablo, J. Chem. Phys. **134**, 194903 (2011).
[66] I. Lyubimov, M. D. Ediger, and J. J. de Pablo, J. Chem. Phys. **139**, 144505 (2013).
[67] P. H. Lin, I. Lyubimov, L. Yu, M. D. Ediger, and J. J. de Pablo, J. Chem. Phys. **140**, 204504 (2014).
[68] J. Helfferich, I. Lyubimov, D. Reid, and J. J. de Pablo, Soft Matter **12**, 5898 (2016).
[69] J. H. Mangalara, M. D. Marvin, and D. S. Simmons, J. Phys. Chem. B **120**, 4861 (2016).
[70] P. Z. Hanakata, J. F. Douglas, and F. W. Starr, Nat. Commun. **5**, 4163 (2014).
[71] R. J. Lang and D. S. Simmons, Macromolecules **46**, 9818 (2013).
[72] K. Paeng, S. F. Swallen, and M. D. Ediger, J. Am. Chem. Soc. **133**, 8444 (2011).
[73] G. S. Grest and K. Kremer, Phys. Rev. A **33**, 3628 (1986).
[74] K. Kremer and G. S. Grest, J. Chem. Phys. **92**, 5057 (1990).
[75] M. Pütz, K. Kremer, and G. S. Grest, Europhys. Lett. **49**, 735 (2000).
[76] S. Peter, H. Meyer, and J. Baschnagel, J. Polym. Sci., Part B: Polym. Phys. **44**, 2951 (2006).
[77] S. Peter, H. Meyer, and J. Baschnagel, J. Chem. Phys. **131**, 14902 (2009).
[78] P. Z. Hanakata, J. F. Douglas, and F. W. Starr, J. Chem. Phys. **137**, 244901 (2012).
[79] W. Gotze and L. Sjogren, Rep. Prog. Phys. **55**, 241 (1999).
[80] J. Dudowicz, K. F. Freed, and J. F. Douglas, Adv. Chem. Phys. **137**, 125 (2008).
[81] S. Plimpton, J. Comput. Phys. **117**, 1 (1995).
[82] R. Jones, S. Kumar, D. Ho, R. Briber, and T. Russell, Nature **400**, 146 (1999).
[83] B. O'Shaughnessy and D. Vavylonis, J. Phys.: Condens. Matter **17**, 29 (2004).
[84] W. Kob, F. Sciortino, and P. Tartaglia, Europhys. Lett. **49**, 590 (2000).
[85] P. Scheidler, W. Kob, and K. Binder, Europhys. Lett. **59**, 701 (2002).
[86] D. S. Simmons, Macromol. Chem. Phys. **217**, 137 (2016).
[87] H. Zhang, Y. Yang, and J. F. Douglas, J. Chem. Phys. **142**, 084704 (2015).
[88] Y. Sun, L. Zhu, K. L. Kearns, M. D. Ediger, and L. Yu, Proc. Natl. Acad. Sci. U. S. A. **108**, 5990 (2011).
[89] L. Zhu, C. W. Brian, S. F. Swallen, P. T. Straus, M. D. Ediger, and L. Yu, Phys. Rev. Lett. **106**, 256103 (2011).
[90] K. Paeng, R. Richert, and M. D. Ediger, Soft Matter **8**, 819 (2012).
[91] C. W. Brian and L. Yu, J. Phys. Chem. A **117**, 13303 (2013).
[92] C. Donati, S. C. Glotzer, P. H. Poole, W. Kob, and S. J. Plimpton, Phys. Rev. E **60**, 3107 (1999).
[93] W. Kob, C. Donati, S. J. Plimpton, P. H. Poole, and S. C. Glotzer, Phys. Rev. Lett. **79**, 2827 (1997).
[94] C. Donati, J. F. Douglas, W. Kob, S. J. Plimpton, P. H. Poole, and S. C. Glotzer, Phys. Rev. Lett. **80**, 2338 (1998).
[95] F. W. Starr, J. F. Douglas, and S. Sastry, J. Chem. Phys. **138**, 12A541 (2013); e-print arXiv:1302.5029v1.
[96] F. W. Starr and J. F. Douglas, Phys. Rev. Lett. **106**, 115702 (2011).
[97] B. A. Pazmiño Betancourt, J. F. Douglas, and F. W. Starr, J. Chem. Phys. **140**, 204509 (2014).
[98] B. A. Pazmio Betancourt, P. Z. Hanakata, F. W. Starr, and J. F. Douglas, Proc. Natl. Acad. Sci. U. S. A. **112**, 2966 (2015).
[99] R. A. Riggleman, K. Yoshimoto, J. F. Douglas, and J. J. de Pablo, Phys. Rev. Lett. **97**, 045502 (2006).
[100] M. Aichele, Y. Gebremichael, F. Starr, J. Baschnagel, and S. Glotzer, J. Chem. Phys. **119**, 5290 (2003).
[101] W. Kob and H. C. Andersen, Phys. Rev. E **52**, 4134 (1995).